

# Absorbing State Phase Transition with Clifford Circuits

Nastasia Makki,\* Nicolai Lang, and Hans Peter Büchler

*Institute for Theoretical Physics III and Center for Integrated Quantum Science and Technology,  
University of Stuttgart, 70550 Stuttgart, Germany*

(Dated: March 10, 2023)

The role of quantum fluctuations in modifying the critical behavior of non-equilibrium phase transitions is a fundamental but unsolved question. In this study, we examine the absorbing state phase transition of a 1D chain of qubits undergoing a contact process that involves both coherent and classical dynamics. We adopt a discrete-time quantum model with states that can be described in the stabilizer formalism, and therefore allows for an efficient simulation of large system sizes. The extracted critical exponents indicate that the absorbing state phase transition of this Clifford circuit model belongs to the directed percolation universality class. This suggests that the inclusion of quantum fluctuations does not necessarily alter the critical behavior of non-equilibrium phase transitions of purely classical systems. Finally, we extend our analysis to a non-Clifford circuit model, where a tentative scaling analysis in small systems reveals critical exponents that are also consistent with the directed percolation universality class.

## I. INTRODUCTION

Non-equilibrium quantum phase transitions are interesting because they can exhibit universal behavior that is distinct from classical systems [1, 2], but are in general much harder to study. Recently, quantum contact models have been proposed as promising systems to explore this possibility [3]. Classical contact models are among the conceptually simplest to investigate non-equilibrium phase transitions. They are characterized by the competition of a spreading mechanism and a probabilistic decay, and are widely utilized in describing phenomena like the spread of diseases, forest fires and bacteria colonies [4–8]. For a low spreading rate, the system reaches a state with no infected units and remains stuck in this absorbing state. However, as the spreading rate increases beyond a critical value, the system reaches an active state where the density of infected units fluctuates around a fixed finite value. The phase transition in classical contact processes is well understood: it falls under the directed percolation (DP) universality class, and all critical exponents are known to high precision [9]. Quantum analogs of contact processes, on the other hand, remain less well understood. Since the computational capacities of classical computers limit the exact simulation of generic many-body quantum systems to small sizes, many questions concerning their quantum critical behavior remain unanswered. Here, we study the critical properties of an absorbing state phase transition in a random quantum circuit model based on Clifford operations, which can be efficiently studied numerically.

The study of quantum contact processes has been motivated by a potential experimental realization with Rydberg atoms [10]. Such neutral atoms, excited to Rydberg states and individually trapped by optical tweezers or in the frozen regime, have emerged as a highly promising platform for the quantum simulation of equilibrium

and non-equilibrium quantum many-body systems [11–20]. The interplay of coherent driving, strong interactions between the Rydberg states, and spontaneous decay also opens the possibility to explore models closely related to quantum contact processes [21]. Convenient observables, such as population loss and excitation density, display power-law scaling with the driving strength, and the inferred exponents provide insight into the critical behavior of such systems [22]. First theoretical studies using a mean-field approach suggest a first order transition for the pure quantum contact model, and including classical contributions leads to the existence of a bicritical point, for which the universal behavior deviates from the classical continuous DP transition [3, 10]. A renormalization group analysis concludes that strong temporal and spatial fluctuations in the active phase smooths out the first order transition predicted by mean-field approximations [23]. Numerical simulations of a 50 site chain using a tensor network (iTEBD) algorithm report a continuous absorbing state phase transition and provide first estimates for the critical exponents of a new quantum contact universality class [24–26]. A machine learning approach, employed to pinpoint the critical region, followed by a tensor network and quantum jump Monte Carlo analysis also provide estimates for the critical exponents [27]; they find that only one (decay) exponent differs from the DP value, and only in the case where the system is initialized in a homogeneous, all active state. In general, numerical methods are strongly limited by the size of the system they allow to simulate [28]. The finite bond dimension of tensor networks limits this method to systems with low entanglement, another obstacle that makes accurate studies of critical quantum behavior challenging. However, there are alternative numerical methods based on stabilizer states which allow for the exploration of quantum systems with extensive entanglement. Such Clifford quantum circuits can simulate unitary as well as dissipative operations, and can be efficiently implemented on classical computers [29]. This approach has recently been successfully applied to investigate entanglement transitions [30–33].

\* [nastasia.makki@itp3.uni-stuttgart.de](mailto:nastasia.makki@itp3.uni-stuttgart.de)

In this manuscript, we study a quantum circuit version of a contact process based on Clifford operations. As universal properties are independent of the microscopic realization, we expect a critical behavior that can also be realized in continuous time quantum contact models. At each discrete time step we apply with some probability a set of unitary gates to represent coherent time dynamics, and some projective measurements to simulate dissipative decay. More importantly, we restrict the gates to the Clifford group of unitaries, which restricts the Hilbert space and thus allows for the efficient simulation of the system near its thermodynamic limit. Our results show that contact process transitions simulated with Clifford circuits belong to the directed percolation universality class. We observe that keeping the absorbing state dynamically stable, while restricting the Hilbert space to stabilizer states, leads to steady states with limited entanglement at the phase transition as well as in the active phase. The quantum effects included in this approach are insufficient to change the universality class of the classical contact process. To check if abandoning the Clifford restriction causes a distinctive change to the dynamics, we introduce a non-Clifford quantum contact process and study its non-equilibrium properties on a small system of 20 qubits. The data suggests a volume law entanglement scaling in the active phase of this non-Clifford quantum contact model. Because of the strong finite size effects, we cannot reliably extract critical exponents from the exact simulation data. However, if we assume for the critical exponents the values of DP, we find that the scaling behavior for small systems is still consistent with this assumption. These inconclusive results emphasize the importance of realizing such models on emerging quantum simulation platforms where larger systems can be analysed.

## II. MODEL

We focus on a 1D lattice of length  $L$  with periodic boundaries. Each site is a two-level quantum system represented by a qubit state. The basis states are labeled  $|1\rangle$  and  $|0\rangle$  which we translate to contact process language as  $|\text{active}\rangle$  and  $|\text{inactive}\rangle$  states respectively. At each time step, a set of dynamical rules apply which define how activation can spread and coagulate within a system. The simplest classical contact process requires two dynamical rules. First, sites can become active if and only if one of their nearest neighbors is already in an active state, i.e., by contact. Second, active sites can spontaneously decay and become inactive. Spontaneous activation should be impossible which makes the state where all the sites are inactive invariant under the dynamical rules. Therefore, once a system ends up in the fully inactive state, it gets stuck in this state which is therefore termed *absorbing*. The other dynamically stable state of this system is when the spreading and decay processes balance each other such the density of active sites fluctuates around a finite fixed value. The system is then said to be in an *active*

*phase*. The relative strength of the spreading probability and decay probability determine the steady state and changing it drives a phase transition. The presence of an absorbing state violates detailed balance, making this transition an out-of-equilibrium phase transition. In a classical system, the sites can only exist in one of the two basis states, either active or inactive. The classical phase transition is well studied and classified into the directed percolation (DP) universality class; for a detailed review on the classical contact process we refer the reader to [9].

To investigate quantum analogs of this phase transition, we map the problem to a discrete time quantum circuit where unitary gates and measurements are chosen to reproduce the dynamical rules of a contact process applied now to a chain of qubits. In this paper, we study two models that implement the ideas of the contact process in a quantum system. The first is a Clifford model where we restrict the gates to the set of Clifford unitaries: Hadamard (H), Controlled-Not (CNOT), and Phase (P) gates. Operations that can be written in terms of the Clifford set are also included such as the Pauli matrices: X, Y and Z. In the second model, we relax this restriction. Fig. 1 shows the dynamical rules applied by the different activation spreading operations in our two models. The decay operation is the same for both models; it is achieved via a projective single site measurement onto the Z-basis followed by a flip using the X gate if the measurement result was an active site. This operation is applied on each site with a constant probability  $\gamma$ .

In the Clifford model, activation is spread via layers of CNOT gates, each applied with a probability  $\omega$ , and via layers of Cond $\sqrt{X}$  operations, each applied with a probability  $\kappa$ . The conditioned- $\sqrt{X}$  operation is defined to first *measure* the control qubit and only if the measurement yields the control qubit in the active state, apply a  $\sqrt{X}$  gate on the target qubit. We start with the simplest Clifford contact model where  $\kappa = 0$ . This model is referred to as the CNOT model. At a fixed decay rate  $\gamma = 0.1$ , varying the spreading coupling  $\omega$  drives the system through an absorbing state phase transition. The analysis of the critical point is shown in Fig. 8 (Appendix A), where the scaling behavior is found to fall into the directed percolation (DP) universality class. The equivalence of the CNOT model to a classical contact model can be easily seen if one considers initializing the system in a product state of sites in the Z-basis, i.e., a classical state. The dynamical rules dictate that the system remains in such a classical state as entangled states can be created only if the control site of the applied CNOT gate happens to be in a superposition of the basis states. Therefore, to observe a finite entanglement entropy of a chosen subsystem with the rest, we should start our simulations with a state where some sites are not in the Z-basis. However, the decay operation continuously removes entanglement and we find that for any finite  $\gamma$ , the system eventually converges to a classical product state where sites are either active or inactive. A similar result is obtained if one considers the Clifford model with  $\omega = 0$  and  $\kappa > 0$  which we refer to as

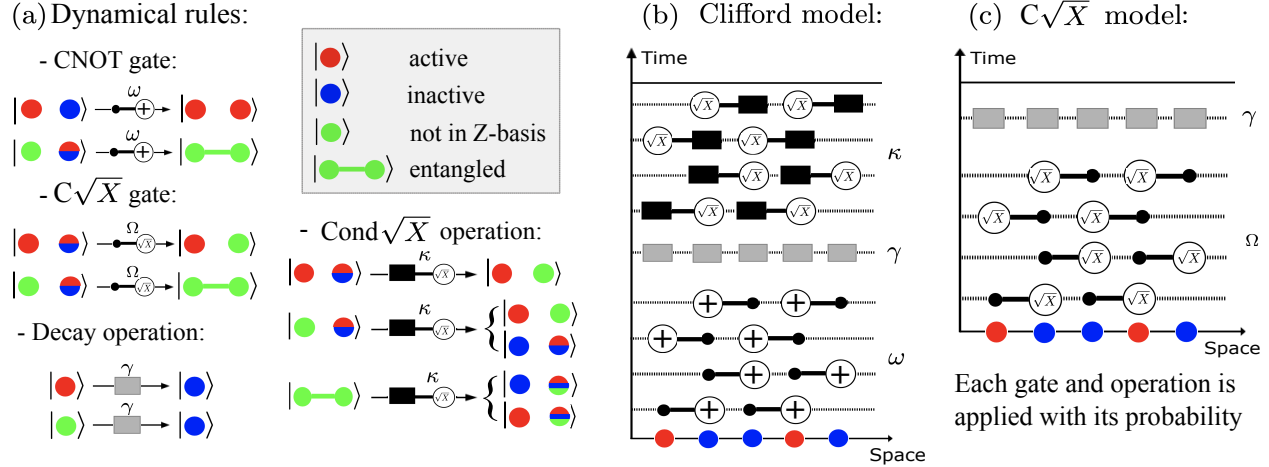


Figure 1. **Quantum contact models.** The basis states  $|\bullet\rangle = |\text{active}\rangle$  and  $|\bullet\rangle = |\text{inactive}\rangle$  are eigenstates of the Pauli operator  $Z$ .  $|\bullet\rangle$  represents a site that is not in a  $Z$ -eigenstate and  $|\bullet\bullet\rangle$  is a generic entangled state. (a) The dynamical rules: First, the decay operation  $\blacksquare$  is applied with probability  $\gamma$ . It is a single site process where a projective  $Z$ -measurement is performed on the qubit followed by an  $X$  gate to flip the state if the measurement outcome was  $|\text{active}\rangle$ . The CNOT gate  $\bullet\oplus$  is applied with a probability  $\omega$ . The gate can activate an inactive site if the control was active. An entangled state is created if the control is in a superposition. The controlled- $\sqrt{X}$  ( $C\sqrt{X}$ ) gate  $\bullet\sqrt{X}$  is applied with a probability  $\Omega$ . A product state where the control is active leads to the creation of a local superposition on the target site. Another application of the gate activates an initially inactive target. Entangled pair states can be created as well if the control is in a superposition. Finally, we define a two-qubit operation: The conditioned- $\sqrt{X}$  (Cond $\sqrt{X}$ ) gate  $\blacksquare\sqrt{X}$  is applied with a probability  $\kappa$ . The condition is based on a measurement outcome of the control site; if active, the target is acted upon with a  $\sqrt{X}$  gate. This process decoheres an entangled state, but creates a local superposition after being applied to a product state in the  $Z$ -basis. (b) The Clifford model is defined as a quantum circuit that combines layers of CNOT gates and Cond $\sqrt{X}$  operations, applied symmetrically in a checker board manner, with a layer of single site decay operations. The sketch above represents a single time step where each operation is applied with a given probability. For a fixed finite decay probability  $\gamma$ , there exists a critical  $\omega$  and  $\kappa$  below which the system evolves into a dynamically stable absorbing phase defined as all sites are inactive. (c) The  $C\sqrt{X}$  model is defined as a quantum circuit built from layers of  $C\sqrt{X}$  gates and decay operations. We expect to observe an absorbing state phase transition as we increase the probability  $\Omega$  at constant decay  $\gamma$  where the dynamics is dominated by quantum effects. However, this is a non-Clifford circuit which can be numerically simulated only for small system sizes.

the Cond $\sqrt{X}$  model. Increasing  $\kappa$  at a fixed decay rate also drives the system through an absorbing state phase transition within the DP universality class, as shown in Fig. 9 in Appendix A. The critical point occurs at twice the value of the CNOT model which is explained by the fact that for classical states, two conditioned- $\sqrt{X}$  operations are equivalent to a CNOT gate. We expect that the character of the phase transition can change in a quantum circuit where dynamical creation of entanglement entropy is possible, where gates that rotate the local state and not just flip it are used to spread activation. However, if we replace the CNOT with a controlled-Hadamard (CH) or a controlled- $\sqrt{X}$  ( $C\sqrt{X}$ ), the resulting contact models are non-Clifford and thus cannot be simulated efficiently on classical computers. In Section IV we present an analysis of the absorbing state phase transition that occurs in the  $C\sqrt{X}$  model, depicted in Fig. 1c, for a small chain of 20 qubits. In the following, we focus on the Clifford model shown in Fig. 1b. When both probabilities  $\kappa$  and  $\omega$  are finite, entangled states can be created dynamically but require two steps. First, a Cond $\sqrt{X}$  operation is needed to

create a local superposition and then subsequent CNOT gates can spread the entanglement.

### III. RESULTS

Here we present the results for the Clifford model simulation. We initialize the system with half the sites activated, chosen randomly for each realization. The initial state is then evolved by applying the quantum circuit for  $t_s$  time steps; this is repeated for  $10^3$  realizations. The main observable is the average density of active sites  $n(t)$  as a function of time  $t$ ; this quantity depends on the initial state on short timescales but later acquires a behavior independent of the initial condition. The number of applied time steps  $t_s$  for each simulation should be chosen sufficiently long for the system to reach the steady state regime. The density  $n$  of active sites in the steady state is the order parameter of the absorbing state phase transition. It changes from zero in the absorbing phase to a finite value in the active phase. It is important to note that in a finite size simulation, the steady state in the active

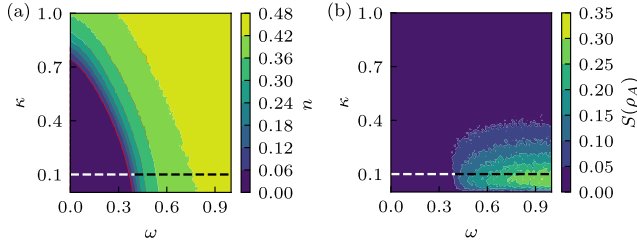


**Figure 2. Phase diagram of the Clifford model.** (a) For a fixed decay constant ( $\gamma = 0.1$ ) we observe an absorbing phase with zero steady state density in the region of small spreading parameters  $\omega \lesssim 0.41$  and  $\kappa \lesssim 0.79$ . (b) Shows the corresponding steady state half-system entanglement entropy. In the absorbing phase and along the axis  $\omega = 0$  and  $\kappa = 0$ , the steady state is a product state so  $S(\rho_A) = 0$ . The entropy decreases with increasing rate of projective measurements given by  $\kappa$ . We focus on the density transition in the region of small but finite  $\kappa$  where we observe a finite entanglement in the active phase.

phase is only quasi-steady; an initial state which evolved into a quasi-steady state remains there for a relatively long time compared to the time needed for equilibration, before eventually decaying into the absorbing state. The lifetime of a quasi-steady state grows exponentially with the size of the considered system. In our simulations, system sizes up to  $L = 400$  sites and  $t_s = 10^4$  time steps are considered. Fig. 2a shows the phase diagram obtained for the Clifford model at constant decay rate  $\gamma = 0.1$ , size  $L = 200$  and a steady state time of  $t_s = 10^2$  steps. The absorbing phase exists for small values of the two spreading couplings  $\omega$  and  $\kappa$ , representing the coherent and incoherent dynamics respectively. The corresponding steady state entanglement entropy  $S(\rho_A)$ , where  $\rho_A$  denotes the subsystem of size  $L_A = L/2$ , is plotted in Fig. 2b. It vanishes in the absorbing phase where all sites are inactive, also in regions where the dynamics ends up in a product state, like on the  $\kappa = 0$  and  $\omega = 0$  axes where states are classical by construction of the model.  $S(\rho_A)$  continuously decreases with increasing  $\kappa$ , as each  $\text{Cond}\sqrt{X}$  operation includes a projective measurement. Therefore, the interesting regime to study the phase transition appears in the region of small  $\kappa$  where  $S(\rho_A)$  is finite in the active phase. We consider the absorbing phase transition along the highlighted line  $\kappa = \gamma = 0.1$ . Fig. 3a shows the change in the order parameter  $n$  as a function of the CNOT rate  $\omega$ . The phase transition is clearly continuous. The scaling analysis, which estimates the critical exponents, shows that all values agree with the known directed percolation exponents that appear in the classical contact process, Fig. 3b-d; see Appendix A for details on the scaling analysis.

This result shows that the classical universality class can persist in a quantum model with dynamically generated entanglement. However, in our Clifford model, the entanglement entropy in the active phase is small and remains in the area law scaling regime.

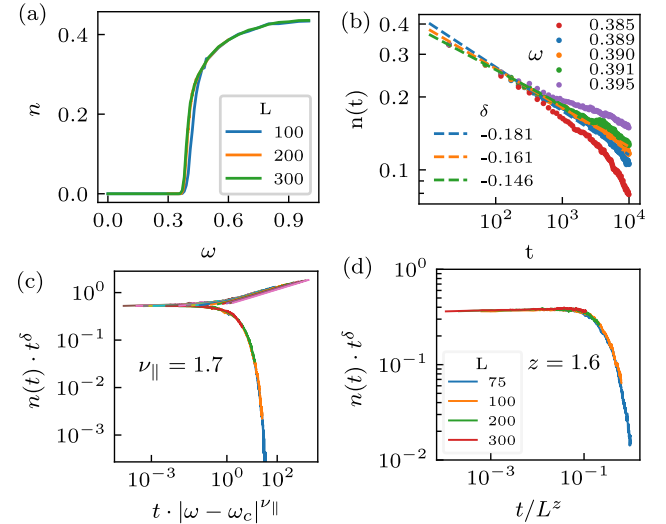


**Figure 3. Scaling analysis of the Clifford model.** (a) At fixed  $\gamma = \kappa = 0.1$ , the order parameter  $n(t_s)$ , the steady state density of active sites, increases continuously from zero as a function of  $\omega$ . (b) The critical point of this second order transition is estimated around  $\omega_c = 0.390$  where  $n(t)$  decays as a power as a function of simulation time. We then deduce the value of the decay exponent  $\delta = 0.161(9)$  from the slope of the fitted straight line in the double logarithmic scale. (c) The best data collapse is obtained for the temporal correlation exponent  $\nu_\parallel = 1.70(3)$ , such that  $\beta = \delta \cdot \nu_\parallel = 0.27(2)$ . (d) Also, near criticality, the data from different sizes collapses into a universal scaling function for  $z = 1.60(3) = \nu_\parallel/\nu_\perp$ , so the spacial correlation exponent is  $\nu_\perp = 1.06(4)$ . All derived exponents are in good agreement with the DP universality class (Table I).

One can try to create more entanglement by increasing the relative effect of creating local superpositions (versus projective measurements) and applying more than one  $\sqrt{X}$  gate per measurement. We refer to these multi-qubit operations as  $\text{Cond}\sqrt{X}\bar{X}$  and  $\text{Cond}\sqrt{X}\bar{X}\bar{X}$ . Such operations can be interpreted in the context of the contact process as an increase in the range of interaction. In Fig. 4 we compare the absorbing state transitions obtained in these models. We observe that despite reaching considerably higher values for the half-system entanglement entropy, the nature of the phase transition remains clearly within the directed percolation universality class. The critical point occurs for lower values of the coupling  $\omega_c$ , which is expected. The scaling analysis is given in Fig. 11 in Appendix B.

We note that in all these cases the entanglement entropy grows from zero continuously when crossing the transition into the active phase and seems that at the critical point, it remains too low to affect the universal behavior.

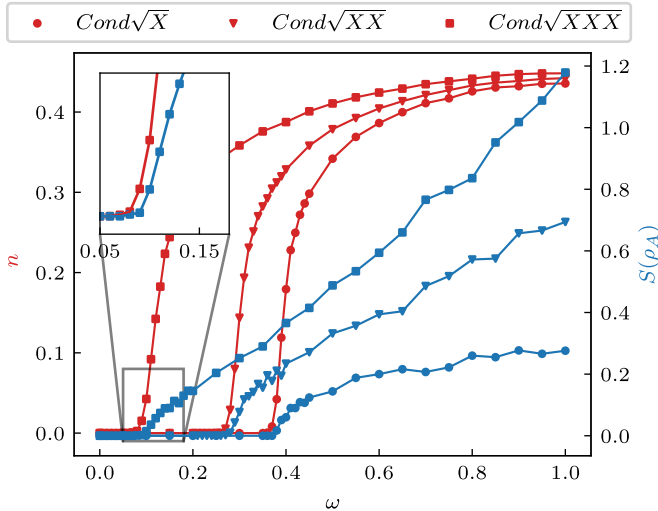


Figure 4. **Increased range of contact.** We replace the  $\text{Cond}\sqrt{X}$  operation in our Clifford model first with  $\text{Cond}\sqrt{XX}$  and then  $\text{Cond}\sqrt{XXX}$ . Simulating the dynamics at the same fixed values for the probabilities  $\gamma = \kappa = 0.1$ , we observe an increase in the values of entanglement entropy reached in the active phase. The nature of the transition to the absorbing phase remains continuous and within the DP universality class. Note that the entanglement also grows continuously from zero and remains small at the transition.

	DP	CNOT	Clifford	$\text{Cond}\sqrt{XXX}$
$\delta$	0.1595	0.161(6)	0.161(9)	0.154(6)
$\beta$	0.2765	0.27(2)	0.27(2)	0.26(2)
$\nu_{\parallel}$	1.7338	1.70(3)	1.70(3)	1.70(3)
$\nu_{\perp}$	1.0969	1.06(4)	1.06(4)	1.06(4)

Table I. **Critical exponents.** The critical behavior of all contact processes within the Clifford formalism is consistent with DP.

#### IV. NON-CLIFFORD MODEL

Now we focus on the non-Clifford  $\text{C}\sqrt{X}$  model. The  $\text{C}\sqrt{X}$  gate is unitary and results in a coherent spreading dynamics and the dynamical creation of entangled states. For a relatively weak rate  $\Omega$  of applying  $\text{C}\sqrt{X}$  gates, a finite decay rate drives the system into a classical absorbing phase, the existence of which is guaranteed by a finite threshold for anisotropic bond percolation on the square lattice [34] (here: the space-time lattice in Fig. 1c). By increasing  $\Omega$ , a transition from the absorbing phase into an active phase is expected. Fig. 5a shows the variation in the normalized density of active sites  $n$  as a function of  $\Omega$  at constant  $\gamma = 0.1$  and the corresponding entanglement entropy  $S(\rho_A)$  obtained after  $t = 100$  steps on a small system of 20 qubits. Simulating for longer times would result in a decay of  $n$  driven by finite size effects, so the steady state regime is hard to capture in such small system sizes. Nevertheless, we observe a key difference with respect to the Clifford models. The entanglement entropy  $S(\rho_A)$  in the active phase reaches much higher

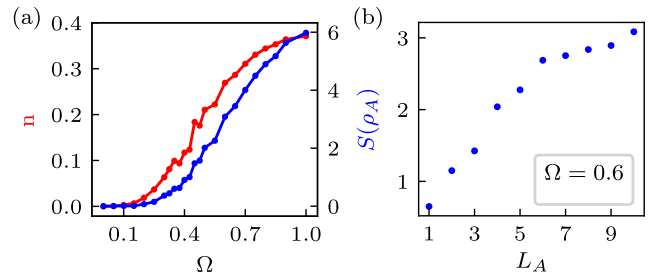


Figure 5. **The  $\text{C}\sqrt{X}$  model.** (a) For a small system of size  $L = 20$  qubits, exact simulations indicate a continuous absorbing state transition where both, the steady state density and the entanglement entropy increase continuously from zero with rate  $\Omega$  at fixed decay rate  $\gamma = 0.1$ . (b) For  $\Omega = 0.6$ , where the system appears to be in the active phase, the entanglement entropy scales with the volume of the subsystem: Plotting  $S(\rho_A)$  versus the size  $L_A$  of subsystem  $A$  shows a linear growth when  $L_A$  is small compared to the full system size. The increase then saturates due to the finite size.

values. It seems to scale as a volume law, indicated by the linear increase of  $S(\rho_A)$  as a function of subsystem size  $L_A$  especially for small  $L_A$  relative to  $L$  as shown in Fig. 5b. On the other hand, and similar to the behavior observed for the Clifford model transition, we find that both  $n$  and  $S(\rho_A)$  increase continuously from zero to finite values as we increase  $\Omega$ , which is consistent with a second order phase transition.

To investigate the finite size effects on this transition, we compare the scaling behavior to that of the CNOT model at an equal size  $L = 20$  but where the universal exponents are all well known, see Fig. 6. The finite size limits the time range for which data can be considered for the scaling analysis. Extracting critical exponents from this data is impossible, we can only check for its consistency with the known DP exponents.

In the case of the CNOT model, the expected critical point  $\omega_c$  and the decay exponent  $\delta$  both fall within the possible critical range observed in the  $L = 20$  simulation data of Fig. 6d. In Fig. 12 (Appendix C) we show data collapse plots for various choices of fitted exponents as well as for the theoretical values of DP exponents while varying the critical point within this range. The quality of this data collapse into the universal scaling functions is consistently better for parameters closer to the results expected from simulating larger chains. Therefore we can conclude that for the CNOT model the  $L = 20$  data fits well with the expected classical DP critical behavior up to simulation times around  $t = 100$  after which finite size effects become dominant.

A similar analysis for the  $\text{C}\sqrt{X}$  model reveals a few notable differences: First, at short times  $t < 10$ , the density of active sites  $n$  fluctuates, an effect mainly observed for simulations with relatively large  $\Omega$  where the system is expected to end up in an active phase. Also finite size effects seem to be stronger, the overall decay in  $n$  starts at earlier simulation time, as seen Fig. 6c. The scaling of

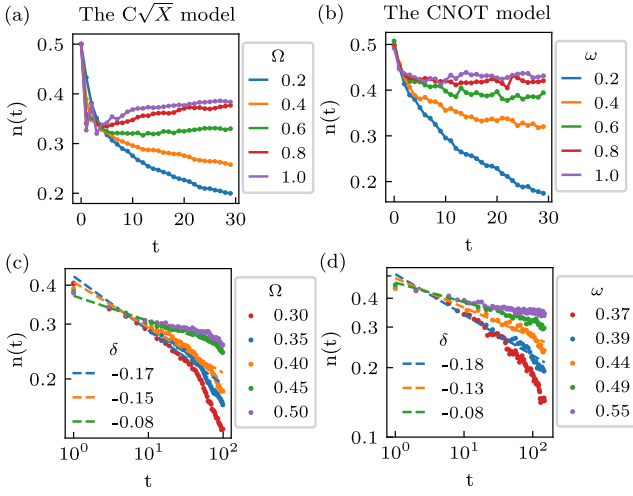


**Figure 6. Comparison of the  $C\sqrt{X}$  and CNOT models.** (a,b) Early time evolution of the order parameter  $n$  in the  $C\sqrt{X}$  and CNOT models, respectively. (c,d) Evolution of  $n$  at later times. From larger systems, we know the critical point  $\omega_c = 0.39$  of the CNOT model; the fitted power law at this point has a 10% error with respect to the expected DP value. We can identify a range for  $\omega_c$  where the decay in  $n$  is linear in logarithmic scale up to  $t = 100$ , after which finite size effects dominate the dynamics. In the  $C\sqrt{X}$  model, at short times we observe fluctuations in  $n$  for larger  $\Omega$ . Another distinctive feature of the  $C\sqrt{X}$  model is that  $n(t)$  smooths out to a lower average value compared to that of the CNOT transition at similar coupling strength. Also finite size effects (in the form of overall decay of  $n$ ) occur earlier than  $t = 100$  steps. Despite the clear differences, we cannot exclude the DP value for the decay exponent  $\delta$ .

the data is analyzed within a range of  $\Omega$  which possibly include the critical value and are shown in Fig. 13 (Appendix C). The collapse is of worse quality compared to the plots obtained with the CNOT model for the same size. If we assume the values of the exponents  $\beta$  and  $\nu_{\parallel}$  to be the literature DP values, we observe the best collapse for  $\Omega_c \approx 0.45$ . In Fig. 7a we plot the collapsed data from  $C\sqrt{X}$  model with the universal collapse function in grey as a reference. Fig. 7b shows that there exists a choice for non-universal factors  $a_p$  and  $a_t$  that leads to data falling on the universal DP scaling function. Non-universal factors are extracted from scaling data at the critical point (see Fig. 10 in Appendix A) which we can not do in the  $C\sqrt{X}$  model. Fig. 7c and Fig. 7d show that in the CNOT model the data agrees with the expected scaling at the critical point despite the clear finite size effects at larger times, where as in the  $C\sqrt{X}$  model the data scaling reveals an inconsistency. As a result, we conclude that the nature of the absorbing state transition in the  $C\sqrt{X}$  model remains inconclusive.

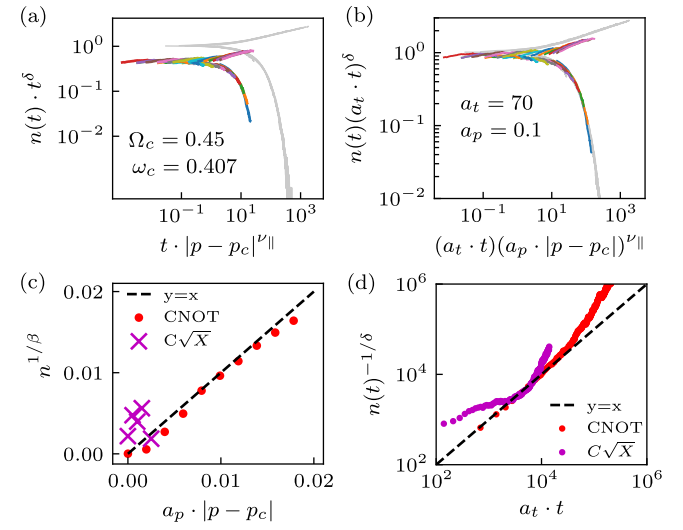


**Figure 7. Consistency with a DP transition.** (a) At  $\Omega_c = 0.45$  we observe the best data collapse in the  $C\sqrt{X}$  model using the known DP critical exponents. The universal DP scaling function is plotted in gray as a reference. (b) We scale the data using non-universal factors  $a_t$  and  $a_p$  such that the scaling functions overlap. In (c) and (d) we check whether at the chosen critical point the data scales as expected with the estimated non-universal factors. For reference we plot the scaled  $L = 20$  data from the CNOT model using non-universal factors derived from the thermodynamic  $L = 400$  system as shown in Fig. 10 (Appendix A). For the  $L = 20$  systems, the data from the CNOT model fits nicely up to large  $t$  when finite size effects dominate. However, the data from the  $C\sqrt{X}$  model doesn't fit the expected scaling behavior.

## V. SUMMARY AND OUTLOOK

We introduced two models of random quantum circuits, comprised of unitary entangling gates and projective measurements, to study the fate of absorbing state phase transitions of classical contact models in the presence of entanglement. The common features of both models are the existence of an absorbing state that is invariant under the time evolution, and a spreading mechanism that allows for the proliferation of excitations in the systems – both necessary ingredients for the occurrence of an absorbing state phase transition. Most importantly, both models feature mechanisms for the *dynamical generation of entanglement*, which distinguishes them from classical contact processes.

The first model – the *Clifford model* – makes use of Clifford gates only and therefore allows for efficient numerical simulations within the stabilizer formalism. With our extensive simulations, we identified an out-of-equilibrium phase transition between an absorbing phase and an active phase. The latter featured low but finite levels of entanglement in certain parameter regimes, which qualifies our model as a *quantum* version of classical contact processes. A scaling analysis revealed critical exponents

that match the directed percolation universality class perfectly. Since the latter also describes the critical behavior of *classical* contact processes, we can conclude that this universality class is robust against certain types of quantum fluctuations.

Since Clifford unitaries only allow for the exploration of a measure-zero subset of the full many-body Hilbert space, their dynamics might be too restrictive to modify this universality class. Our second model – the  $C\sqrt{X}$  model – makes use of the controlled- $\sqrt{X}$  gate to implement both a spreading mechanism and dynamical entanglement generation. This gate is *not* in the Clifford group, and we had to resort to exact evaluations of the time evolution for small system sizes. The simulations revealed signatures of an absorbing state phase transition with significantly stronger entanglement in the active phase. A tentative scaling analysis revealed critical exponents consistent with the directed percolation universality class. However, because of the small system sizes and strong

finite-size effects, our results do not allow for a conclusive characterization of the critical behavior of this process.

Quantum simulations of such non-Clifford models for large systems might be an interesting application for near-term quantum computing platforms. The study of universal features is promising because these are expected to be independent of microscopic details, and therefore might tolerate certain types of noise and gate infidelities of NISQ devices. On the theoretical side, it is an interesting question whether Clifford circuits in general are too restrictive to describe non-classical critical behavior, and whether the numerical study of quantum criticality in non-equilibrium settings is an inherently hard problem.

## ACKNOWLEDGMENTS

This project has received funding from the German Federal Ministry of Education and Research (BMBF) under the grants QRydDemo and MUNIQC-Atoms.

---

[1] L. M. Sieberer, M. Buchhold and S. Diehl, *Keldysh field theory for driven open quantum systems*, Reports on Progress in Physics **79**(9), 096001 (2016), doi:[10.1088/0034-4885/79/9/096001](https://doi.org/10.1088/0034-4885/79/9/096001).

[2] L. M. Sieberer, S. D. Huber, E. Altman and S. Diehl, *Dynamical critical phenomena in driven-dissipative systems*, Phys. Rev. Lett. **110**, 195301 (2013), doi:[10.1103/PhysRevLett.110.195301](https://doi.org/10.1103/PhysRevLett.110.195301).

[3] M. Marcuzzi, M. Buchhold, S. Diehl and I. Lesanovsky, *Absorbing state phase transition with competing quantum and classical fluctuations*, Physical review letters **116**(24), 245701 (2016), doi:[10.1103/PhysRevLett.116.245701](https://doi.org/10.1103/PhysRevLett.116.245701).

[4] D. Mollison, *Spatial contact models for ecological and epidemic spread*, Journal of the Royal Statistical Society: Series B (Methodological) **39**(3), 283 (1977), doi:[10.1111/j.2517-6161.1977.tb01627.x](https://doi.org/10.1111/j.2517-6161.1977.tb01627.x).

[5] P. Grassberger, *On the critical behavior of the general epidemic process and dynamical percolation*, Mathematical Biosciences **63**(2), 157 (1983), doi:[10.1016/0025-5564\(82\)90036-0](https://doi.org/10.1016/0025-5564(82)90036-0).

[6] O. Diekmann and J. A. P. Heesterbeek, *Mathematical epidemiology of infectious diseases: model building, analysis and interpretation*, vol. 5, John Wiley & Sons (2000).

[7] A. L. Sullivan, *Wildland surface fire spread modelling, 1990–2007. 3: Simulation and mathematical analogue models*, International Journal of Wildland Fire **18**(4), 387 (2009), doi:[10.1071/WF06144](https://doi.org/10.1071/WF06144).

[8] J. A. Bonachela, C. D. Nadell, J. B. Xavier and S. A. Levin, *Universality in bacterial colonies*, Journal of Statistical Physics **144**, 303 (2011), doi:[10.1007/s10955-011-0179-x](https://doi.org/10.1007/s10955-011-0179-x).

[9] H. Hinrichsen, *Non-equilibrium critical phenomena and phase transitions into absorbing states*, Advances in physics **49**(7), 815 (2000), doi:[10.1080/00018730050198152](https://doi.org/10.1080/00018730050198152).

[10] M. Buchhold, B. Everest, M. Marcuzzi, I. Lesanovsky and S. Diehl, *Nonequilibrium effective field theory for absorbing state phase transitions in driven open quantum spin systems*, Phys. Rev. B **95**, 014308 (2017), doi:[10.1103/PhysRevB.95.014308](https://doi.org/10.1103/PhysRevB.95.014308).

[11] H. Weimer, M. Müller, I. Lesanovsky, P. Zoller and H. P. Büchler, *A rydberg quantum simulator*, Nature Physics **6**(5), 382 (2010), doi:[10.1038/nphys1614](https://doi.org/10.1038/nphys1614).

[12] M. Saffman, T. G. Walker and K. Mølmer, *Quantum information with rydberg atoms*, Rev. Mod. Phys. **82**, 2313 (2010), doi:[10.1103/RevModPhys.82.2313](https://doi.org/10.1103/RevModPhys.82.2313).

[13] J. Zeiher, R. Van Bijnen, P. Schauß, S. Hild, J.-y. Choi, T. Pohl, I. Bloch and C. Gross, *Many-body interferometry of a rydberg-dressed spin lattice*, Nature Physics **12**(12), 1095 (2016), doi:[10.1038/nphys3835](https://doi.org/10.1038/nphys3835).

[14] H. Bernien, S. Schwartz, A. Keesling, H. Levine, A. Omran, H. Pichler, S. Choi, A. S. Zibrov, M. Endres, M. Greiner *et al.*, *Probing many-body dynamics on a 51-atom quantum simulator*, Nature **551**(7682), 579 (2017), doi:[10.1038/nature24622](https://doi.org/10.1038/nature24622).

[15] N. Šibalić and C. S. Adams, *Rydberg physics*, IOP Publishing, doi:[10.1088/978-0-7503-1635-4](https://doi.org/10.1088/978-0-7503-1635-4) (2018).

[16] H. Kim, Y. Park, K. Kim, H.-S. Sim and J. Ahn, *Detailed balance of thermalization dynamics in rydberg-atom quantum simulators*, Phys. Rev. Lett. **120**, 180502 (2018), doi:[10.1103/PhysRevLett.120.180502](https://doi.org/10.1103/PhysRevLett.120.180502).

[17] S. De Léséleuc, V. Lienhard, P. Scholl, D. Barredo, S. Weber, N. Lang, H. P. Büchler, T. Lahaye and A. Browaeys, *Observation of a symmetry-protected topological phase of interacting bosons with rydberg atoms*, Science **365**(6455), 775 (2019), doi:[10.1126/science.aav9105](https://doi.org/10.1126/science.aav9105).

[18] A. Browaeys and T. Lahaye, *Many-body physics with individually controlled rydberg atoms*, Nature Physics **16**(2), 132 (2020), doi:[10.1038/s41567-019-0733-z](https://doi.org/10.1038/s41567-019-0733-z).

[19] R. Verresen, M. D. Lukin and A. Vishwanath, *Prediction of toric code topological order from rydberg blockade*, Phys. Rev. X **11**, 031005 (2021), doi:[10.1103/PhysRevX.11.031005](https://doi.org/10.1103/PhysRevX.11.031005).

[20] G. Semeghini, H. Levine, A. Keesling, S. Ebadi, T. T. Wang, D. Bluvstein, R. Verresen, H. Pichler, M. Kalinowski, R. Samajdar *et al.*, *Probing topological spin liquids on a programmable quantum simulator*, *Science* **374**(6572), 1242 (2021), doi:[10.1126/science.abi8794](https://doi.org/10.1126/science.abi8794).

[21] T. Wintermantel, M. Buchhold, S. Shevate, M. Morgado, Y. Wang, G. Lochead, S. Diehl and S. Whitlock, *Epidemic growth and griffiths effects on an emergent network of excited atoms*, *Nature Communications* **12**(1), 1 (2021), doi:[10.1038/s41467-020-20333-7](https://doi.org/10.1038/s41467-020-20333-7).

[22] S. Helmrich, A. Arias and S. Whitlock, *Uncovering the nonequilibrium phase structure of an open quantum spin system*, *Physical Review A* **98**(2), 022109 (2018), doi:[10.1103/PhysRevA.98.022109](https://doi.org/10.1103/PhysRevA.98.022109).

[23] D. Roscher, S. Diehl and M. Buchhold, *Phenomenology of first-order dark-state phase transitions*, *Physical Review A* **98**(6), 062117 (2018), doi:[10.1103/PhysRevA.98.062117](https://doi.org/10.1103/PhysRevA.98.062117).

[24] E. Gillman, F. Carollo and I. Lesanovsky, *Numerical simulation of critical dissipative non-equilibrium quantum systems with an absorbing state*, *New Journal of Physics* **21**(9), 093064 (2019), doi:[10.1088/1367-2630/ab43b0](https://doi.org/10.1088/1367-2630/ab43b0).

[25] F. Carollo, E. Gillman, H. Weimer and I. Lesanovsky, *Critical behavior of the quantum contact process in one dimension*, *Physical review letters* **123**(10), 100604 (2019), doi:[10.1103/PhysRevLett.123.100604](https://doi.org/10.1103/PhysRevLett.123.100604).

[26] F. Carollo and I. Lesanovsky, *Nonequilibrium dark space phase transition*, *Physical Review Letters* **128**(4), 040603 (2022), doi:[10.1103/PhysRevLett.128.040603](https://doi.org/10.1103/PhysRevLett.128.040603).

[27] M. Jo, J. Lee, K. Choi and B. Kahng, *Absorbing phase transition with a continuously varying exponent in a quantum contact process: A neural network approach*, *Phys. Rev. Res.* **3**, 013238 (2021), doi:[10.1103/PhysRevResearch.3.013238](https://doi.org/10.1103/PhysRevResearch.3.013238).

[28] H. Weimer, A. Kshetrimayum and R. Orús, *Simulation methods for open quantum many-body systems*, *Rev. Mod. Phys.* **93**, 015008 (2021), doi:[10.1103/RevModPhys.93.015008](https://doi.org/10.1103/RevModPhys.93.015008).

[29] S. Aaronson and D. Gottesman, *Improved simulation of stabilizer circuits*, *Phys. Rev. A* **70**, 052328 (2004), doi:[10.1103/PhysRevA.70.052328](https://doi.org/10.1103/PhysRevA.70.052328).

[30] Y. Li, X. Chen and M. P. A. Fisher, *Quantum zeno effect and the many-body entanglement transition*, *Phys. Rev. B* **98**, 205136 (2018), doi:[10.1103/PhysRevB.98.205136](https://doi.org/10.1103/PhysRevB.98.205136).

[31] B. Skinner, J. Ruhman and A. Nahum, *Measurement-induced phase transitions in the dynamics of entanglement*, *Phys. Rev. X* **9**, 031009 (2019), doi:[10.1103/PhysRevX.9.031009](https://doi.org/10.1103/PhysRevX.9.031009).

[32] A. Chan, R. M. Nandkishore, M. Pretko and G. Smith, *Unitary-projective entanglement dynamics*, *Phys. Rev. B* **99**, 224307 (2019), doi:[10.1103/PhysRevB.99.224307](https://doi.org/10.1103/PhysRevB.99.224307).

[33] Y. Li, X. Chen and M. P. A. Fisher, *Measurement-driven entanglement transition in hybrid quantum circuits*, *Phys. Rev. B* **100**, 134306 (2019), doi:[10.1103/PhysRevB.100.134306](https://doi.org/10.1103/PhysRevB.100.134306).

[34] S. Redner and H. E. Stanley, *Anisotropic bond percolation*, *Journal of Physics A: Mathematical and General* **12**(8), 1267 (1979), doi:[10.1088/0305-4470/12/8/021](https://doi.org/10.1088/0305-4470/12/8/021).

[35] J.-P. Bouchaud and A. Georges, *Anomalous diffusion in disordered media: statistical mechanisms, models and physical applications*, *Physics reports* **195**(4-5), 127 (1990), doi:[10.1016/0370-1573\(90\)90099-N](https://doi.org/10.1016/0370-1573(90)90099-N).

## Appendix A: Scaling theory

Here we discuss the scaling analysis, based on Ref. [9], which describes how we estimate the critical exponents. Absorbing states phase transitions studied in this paper are continuous, second order transitions which are often characterized by universal scaling laws. Different physical systems that exhibit equal sets of critical exponents and coinciding scaling functions belong to the same universality class. A universality class is insensitive to microscopic details of its systems, and usually depends only on properties like dimension, range of interactions, and symmetries. The same picture exists in out-of-equilibrium processes. Most notably, the directed percolation (DP) universality class is labeled by the triplet  $(\beta, \nu_{\parallel}, \nu_{\perp})$  of critical exponents; all other exponents can be deduced from this set using scaling relations. Remark that, in contrast to equilibrium critical phenomena, the dimension of “time” has a different character than the “space” dimension, and we distinguish these by using the indices  $\parallel$  for time and  $\perp$  for space. Contact processes produce an absorbing state phase transition which belong to the DP universality class. The order parameter  $n(t_s)$  is the normalized steady state density of active sites

$$n(t_s) = \left\langle \frac{1}{L} \sum_i n_i(t_s) \right\rangle,$$

where  $\langle \dots \rangle$  is an ensemble average over many realizations,  $L$  is the total number of sites in the system, and  $n_i(t)$  is the local occupation at site  $i$  at time  $t$ . In the thermodynamic limit and close to the transition, the steady state density obeys the scaling

$$n(t_s) \sim |p - p_c|^\beta,$$

where  $p$  is the driving parameter of the transition and  $p_c$  is its critical value. The exponent  $\beta$  is conventionally associated to the scaling of the order parameter, which is the density of active sites in contact process transitions. The spatial correlation length  $\xi_{\perp}$  and the temporal correlation length  $\xi_{\parallel}$  also diverge near criticality with the scaling laws

$$\xi_{\perp} \sim |p - p_c|^{-\nu_{\perp}} \quad \text{and} \quad \xi_{\parallel} \sim |p - p_c|^{-\nu_{\parallel}},$$

where the length scales are related through the dynamical critical exponent  $z = \nu_{\parallel}/\nu_{\perp}$ , defined as  $\xi_{\parallel} \sim \xi_{\perp}^z$ . Those length scales can be determined from their intuitive physical interpretations. For example,  $\xi_{\parallel}$  represents the average decay time of clusters that spread from an initial seed in the absorbing phase, while  $\xi_{\perp}$  represents the average spatial width of such clusters. Although the set  $(\beta, \nu_{\parallel}, \nu_{\perp})$  can be already estimated from the relations above by plotting the associated quantities  $(n(t_s), \xi_{\perp}, \xi_{\parallel})$  in the double logarithmic scale as a function of  $\Delta = |p - p_c|$  and extracting the slope of the resulting straight lines, this estimate is known to be quite inaccurate since the equilibration time to reach the stationary state grows rapidly

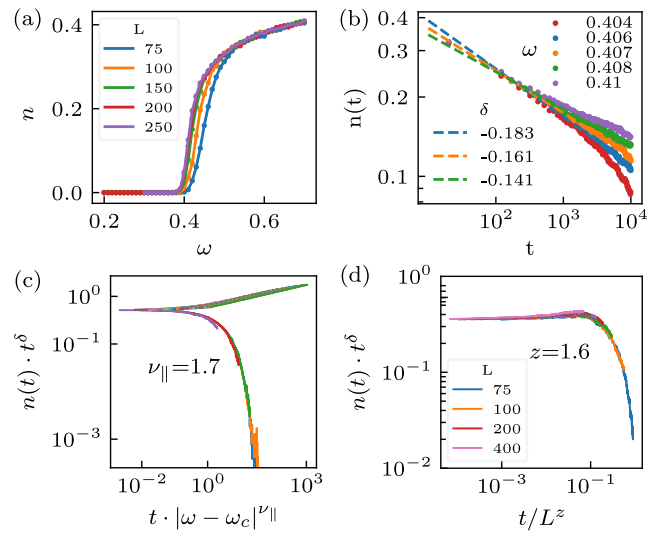


Figure 8. **The CNOT model.** (a) Continuous change in the steady state density  $n$  as a function of  $\omega$  and fixed decay rate  $\gamma = 0.1$  for different system sizes. (b) Power law decay of the order parameter  $n$  as a function of the simulation time. The critical point is estimated at  $\omega_c = 0.4070(5)$ , the slope of the fitted line is 0.16087 which gives the estimate for the critical exponent  $\delta = 0.161(6)$  (consistent with the best known estimate  $\delta_{\text{DP}} = 0.159$  [9]). The other critical exponents are deduced from the collapse plots (c) and (d). All values are compatible with the literature values of the DP transitions.

as the critical point is approached, an effect known as *critical slowing down*. A more accurate approach to extract the critical exponents is to plot the universal scaling functions instead.

Consider the density scaling relation for a finite size system with  $N = L^d$  sites where  $d$  is the spatial dimension:

$$n(t) \sim t^{-\delta} f(\Delta \cdot t^{1/\nu_{\parallel}}, t^{d/z}/N).$$

$f$  has the same functional form for all phase transitions in the DP universality class and can depend only on scale-invariant ratios. Note that a scaling transformation  $x \rightarrow \Lambda x$  of lengths  $x$  is accompanied by rescaling of  $t \rightarrow \Lambda^z t$ ,  $\Delta \rightarrow \Lambda^{-1/\nu_{\perp}} \Delta$  and  $n \rightarrow \Lambda^{-\beta/\nu_{\perp}} n$ . In the thermodynamic limit  $N \rightarrow \infty$ , the universal function  $f$  tends to a constant. Therefore, the exponent  $\delta$  describes the power law decay of the order parameter near criticality  $\Delta \rightarrow 0$ . At large arguments  $\zeta$ ,  $f(\zeta) \rightarrow \zeta^{\delta \cdot \nu_{\parallel}}$ . Therefore in the steady state, as  $t \rightarrow \infty$  we find the scaling relation

$$\beta = \delta \cdot \nu_{\parallel}.$$

Now we apply this analysis to the data obtained from the simulations of the CNOT model. We first plot the order parameter  $n(t_s)$  as a function of the rate  $\omega$  for increasing system sizes and illustrate the continuous nature of the phase transition in Fig. 8a. Then we identify the critical point using the expected asymptotic power law decay of the order parameter  $n(t) \sim t^{-\delta}$  for a sufficiently

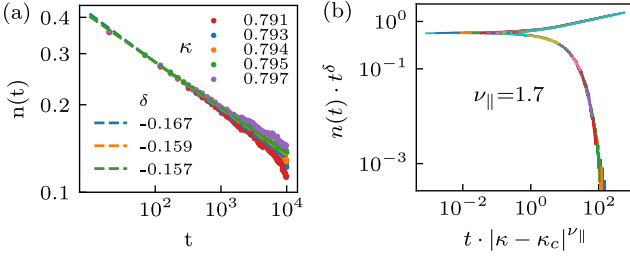


Figure 9. **The Cond $\sqrt{X}$  model.** We observe that the scaling behavior is consistent with the expected classical DP universality class. The data shown is for the system size  $L = 400$  and  $\kappa_c = 0.7940(5)$  is the estimated critical point. The critical exponents are then  $\delta = 0.159(3)$ ,  $\nu_{\parallel} = 1.70(3)$ , and  $\beta = 0.27(1)$  (cf. Table I).

large system of  $L = 400$  sites and long simulation times  $t_s = 10^4$ . Plotting the data in the double logarithmic scale results in a positive (negative) curvature at large  $t$  for coupling  $\omega$  corresponding to the active (absorbing) phase as shown in Fig. 8b. The critical exponent  $\delta$  is then the slope of the best data fit to a straight line. Our estimate for the critical point is  $\omega = 0.407$ , where fitting the data into the straightest line gives a slope 0.161. Taking the interval  $\omega \in [0.4065, 0.4075]$ , the data fits to slopes 0.1724 and 0.1601 respectively, which gives an error estimate to  $\delta = 0.161(6)$ . An interval for  $\omega_c$  with range  $\pm 10^{-3}$  overestimates the error on the exponent as  $\omega \in [0.406, 0.4078]$  results in  $\delta = 0.161 \pm 0.01$ . In all the following estimates of the critical exponents we report the overestimated error from data within range  $\pm 10^{-3}$  of the driving parameter.

Next, we plot  $n(t) \cdot t^\delta$  at different values of  $\omega$  as a function of  $t\Delta^{\nu_{\parallel}}$  and varying  $\nu_{\parallel}$  to obtain the best collapse of the data into one universal scaling function.  $\nu_{\parallel} = 1.7$  is the value that gives the best data collapse plot shown in Fig. 8c, whereas increments of 0.05 to  $\nu_{\parallel}$  give clearly worse collapse plots and thus the error on  $\nu$  and  $z$  is estimated as 0.03. Using  $\nu_{\parallel} = 1.70(3)$  and  $\delta = 0.161(6)$ , we estimate the critical exponent  $\beta = \delta \cdot \nu_{\parallel} = 0.27(2)$ . Finally we plot  $n(t) \cdot t^\delta$  at different system sizes  $L$  and  $\omega = \omega_c$  as a function of  $t/L^z$  (here  $d = 1$  and  $N = L$ ). The exponent  $z$  is varied to optimize the collapse. We find  $z = 1.6(3)$  and deduce the last exponent of the triplet  $\nu_{\perp} = \nu_{\parallel}/z = 1.06(4)$ . All the critical exponents agree with the known DP value, see Table I.

A similar analysis is shown in Fig. 9 for the incoherent Cond $\sqrt{X}$  model, which also falls within the DP universality class, as well as for the Clifford model discussed in the main text (Fig. 3). We conclude that all these contact models share the same critical exponents, despite having different activation spreading processes defined by the dynamical rules illustrated in Fig. 1. To prove that they indeed belong to the same universality class, we should also show that the scaling functions  $f$  coincide. Plotting  $n(t)t^\delta$  as a function of  $t\Delta^{\nu_{\parallel}}$  for the three models at the same decay rate  $\gamma$  and system size  $L$  does not

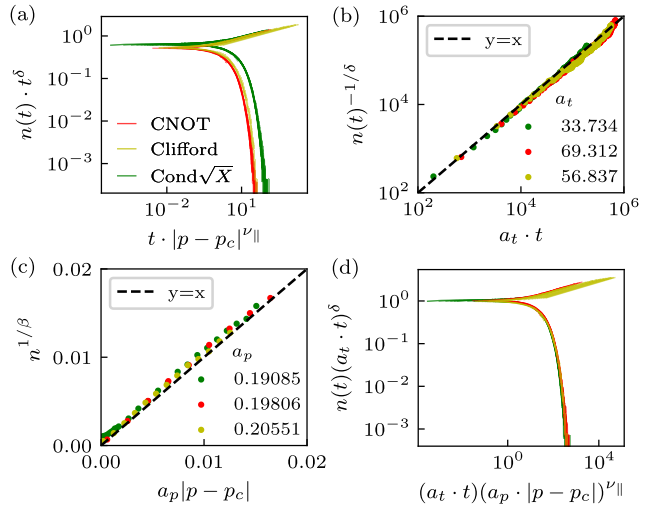
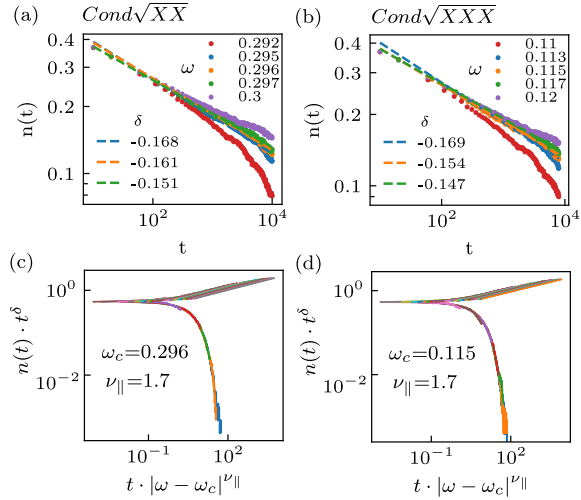


Figure 10. **Non-universal scaling factors.** (a) Collapse plots of the considered models with different spreading gates, where  $p \in \{\omega, \kappa\}$  is the driving parameter of the phase transition. (b,c) Scaling of the simulation data from different models with appropriate factors  $a_p$  and  $a_t$  which encode non-universal microscopic differences specific for each model. (d) Scaled collapse plots which now all fall on top the universal scaling function of the DP class.

show this result (Fig. 10a). However, after scaling the simulation data with appropriate non-universal factors that encode the microscopic properties specific for each model, the scaling functions from the different models indeed collapse to the same universal function, as shown in Fig. 10d. Fig. 10b and Fig. 10c show the results obtained for the non-universal factors  $a_p$  and  $a_t$  respectively. We can estimate these factors by plotting the scaling relations  $n(t_s) = |a_p(p - p_c)|^\beta$  and  $n(t) = a_t t^{-\delta}$  (which are valid near the critical point) in the double logarithmic scales and extract the different slopes corresponding to the data from different models.

## Appendix B: Longer interaction range

Here we discuss the effect of replacing the two-qubit Cond $\sqrt{X}$  operation in the Clifford model with a three-qubit Cond $\sqrt{XX}$  operation or a four-qubit Cond $\sqrt{XXX}$  operation on the nature of the observed absorbing state phase transition. The universality class can depend on the range of interactions. Models where activation spreads over longer distances have been investigated, an example is models with Lévy flight distributions [35]. The universal properties of such processes are known to diverge from that of DP continuously with the control parameter  $\sigma$  which defines the shape of the probability distribution  $P(r) \sim 1/r^{d+\sigma}$  where  $r$  is the distance over which a random interaction can occur; for  $\sigma = \infty$  one gets back the DP case. Contact processes with short-range interaction belong to the DP universality class. In the Clifford models



**Figure 11. Critical exponents for the  $\text{Cond}\sqrt{XX}$  and the  $\text{Cond}\sqrt{XXX}$  models.** (a) We find the exponent  $\delta = 0.161(4)$  at the critical point  $\omega_c = 0.2960(5)$  for the  $\text{Cond}\sqrt{XX}$  model. (c) From the data collapse, we estimate  $\beta = 0.27(1)$ . (b,d) A similar analysis for the  $\text{Cond}\sqrt{XXX}$  model estimates the exponents  $\delta = 0.154(6)$  at  $\omega_c = 0.1150(5)$  and  $\beta = 0.26(2)$ . In both models, the transition remains clearly within the DP universality class, only the transition point shift towards lower spreading rate, which is expected as further sites can be activated by these three and four-qubit operations.

we define, the range of interaction is still short relative to the system size, in particular, it is bounded. So that the nature of the phase transition remains unchanged. This is discussed in Fig. 11 where the obtained critical exponents are still sufficiently close to DP.

### Appendix C: Small system sizes

In this section we investigate how susceptible the data collapse is to variations of the critical exponents for small system sizes. We start with the results of the CNOT model where the critical behavior is known from larger system simulations. For small sizes, the transition point is hard to identify (Fig. 6). Finite size effects dominate the long time regime, we end up with a wide range of spreading rates and corresponding slopes in the logarithmic scale where the decay appears linear. In the  $L = 20$  CNOT model, as shown in Fig. 6, the range appears to be roughly  $0.4 < \omega_c < 0.5$  and  $0.08 < \delta < 0.17$ . Fig. 12a shows the data collapsed with parameters within this range. The error is of the order of the exponent which is expected for such small sizes where extracting exponents from the data is impossible. However, we notice that the  $L = 20$  data collapses nicely on top of the  $L = 300$  data (plotted in gray) when the exponents are close to the expected DP values. This makes us conclude that it is possible, in the case of the CNOT model, to verify the nature of the transition by scaling the simulation data using the known

literature values of the DP exponents. By varying the spreading coupling  $\omega$ , we find an  $\omega_c = 0.42$  where the data shows a good collapse, as seen in Fig. 12b. We remark that a range of values  $\omega \in [0.39, 0.45]$  give relatively good collapse plots, the expected  $\omega_c = 0.407$  is within this interval.

A similar analysis is done on the  $C\sqrt{X}$  model with  $L = 20$ . For this model, the critical behavior is unknown. The collapse plots are shown in Fig. 13, they appear significantly worse than the ones obtained for the CNOT model. However, we cannot exclude a DP transition in the range  $0.4 < \Omega_c < 0.45$  as the upper left most plot and the lower middle plot have a relatively decent collapse quality considering the size limitation.

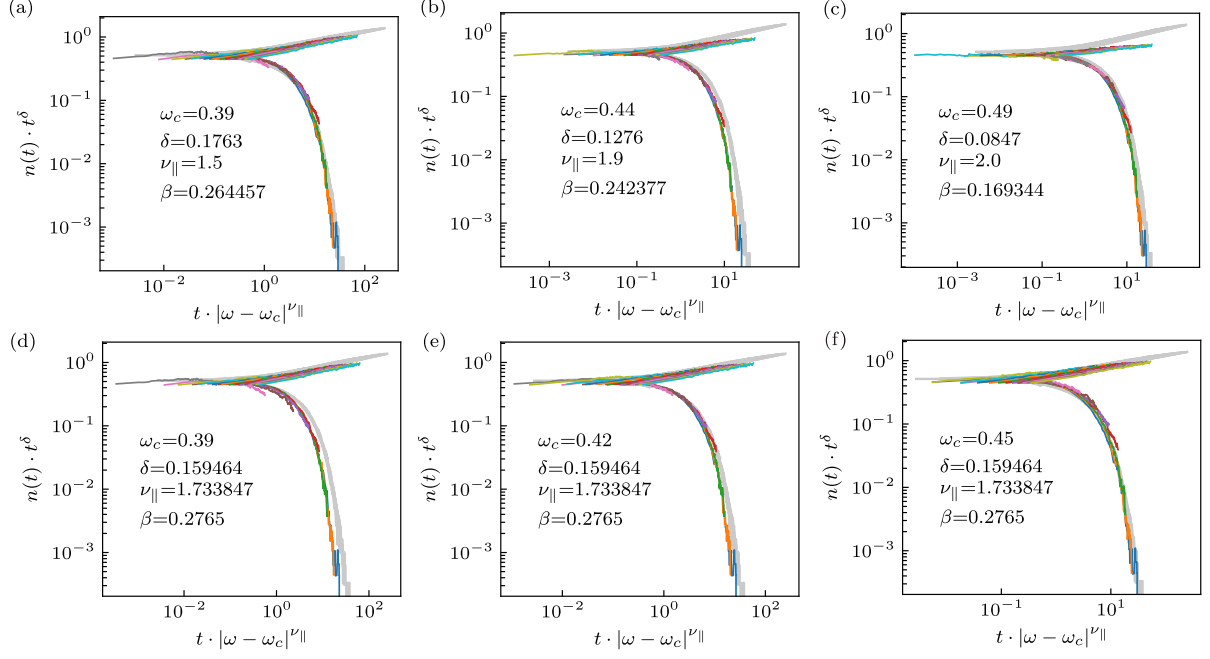


Figure 12. **Collapse plots for the CNOT model at  $L = 20$ .** The large system data is plotted in gray as a background for reference. (a-c) In the upper plots  $\omega_c$  is varied in the range shown in Fig. 6 and  $\delta$  is the fitted exponent. We observe that the data from the  $L=20$  simulation agrees with the thermodynamic results, but at a lower critical value  $\omega_c \approx 0.39$  which is less than  $\omega_c = 0.407$  obtained for  $L = 400$ . (d-f) For the lower collapse plots we fix the literature values for the DP exponents,  $\delta = 0.159$  and  $\nu_{\parallel} = 1.73$ , and vary the critical point  $\omega_c$ . We observe good data collapses within a parameter range  $0.39 < \omega_c < 0.45$ . The best fit occurs around  $\omega_c = 0.42$  which is slightly higher than the thermodynamic value  $\omega_c = 0.407$ .

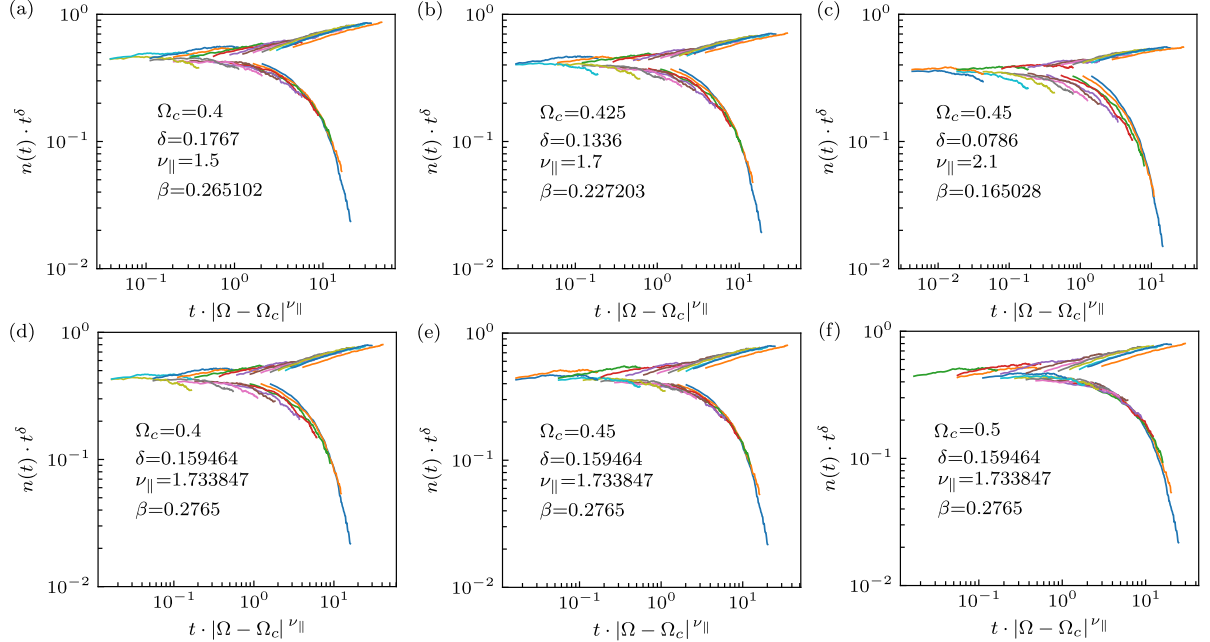


Figure 13. **Collapse plots for  $C\sqrt{X}$  model at  $L=20$ .** We use the data between  $10 < t < 100$  time steps. Plots in (a-c) use fitted  $\delta$  exponents while collapse plots in (d-f) use the DP exponents. Based on this data we cannot exclude a contact process transition within the DP universality class in the  $C\sqrt{X}$  model where the critical point occurs for coupling  $0.4 < \Omega_c < 0.45$ .